Progress In Electromagnetics Research Letters, Vol. 109, 31–39, 2023

Approximate Simulation of Low Frequency Magnetic Shielding of a Rectangular Shielding Box with All Walls Perforated Periodical Holes

Zelai Sun[1], Wei Dong[1], Dingyu Qin[2], Lin Zheng[1], Peng Qiu[3], Chao Ding[3], Xiaochen Yang[2], and Chongqing Jiao[2, *]

Abstract—This article proposes an approximate analytical formulation to calculate the low-frequency magnetic shielding of a rectangular metallic box, with all walls perforated periodical holes. The solution is obtained by the combination of two submodels: the finite conductivity box with the holes covered and the perfect conductor box with the holes present. The first submodel represents the diffusion effect of magnetic field penetration through the conducting shell, and the second one denotes the aperture effect of magnetic field leakage through the holes. The total shielded magnetic field is the superposition of these from the two submodels. For the diffusion effect, an existing empirical formula based on the shape factor is used. To solve the second submodel, we employ two approximate methods: the method of images and the surface-impedance method. The method of images models each hole in the walls as an equivalent magnetic dipole and its images based on Bethe's small aperture coupling theory. A PEC box is first considered. Comparisons with finite element simulations show that the method of images has better accuracy than the surface-impedance method. Then, a cubic aluminum box of 0.2 m in length is treated, which verifies that combining the two submodels can produce results in good agreement with finite element simulations for frequencies up to 10 MHz. In addition, the dependence of the shielding effectiveness on frequency is also analyzed.

1. INTRODUCTION

Low-frequency magnetic shielding has wide applications in many fields, like electric vehicles [1–3], wireless power transmission (WPT) systems [4–6], ultrasensitive atomic sensors [7], and control circuit boards of power electronic devices [8]. Usually, a metallic box is employed as a shielding enclosure. For the solid shield without openings, there are known analytical solutions for a few simple configurations such as infinite plate, infinite cylindrical shell, or spherical shell [9–11].

Frequently, there are some apertures or slots on a shielding enclosure for ventilation or cabling purposes, which can obviously reduce the shielding effectiveness (SE). A shield with a single aperture or a slit or a metallic wire grid has been studied in some papers by applying numerical, analytical, and experimental methods [1, 12–14]. In [14], an analytical model is presented to calculate the low-frequency magnetic SE of a spherical shell with a circular aperture and finite conductivity, which is obtained by the combination of two submodels: enclosed spherical shell with real conductivity and perfect electric conductor (PEC) spherical shell with an aperture. An analytical model is proposed to estimate the low-frequency magnetic field SE prediction of the PEC plate with an array of apertures by magnetization

Received 3 July 2022, Accepted 11 January 2023, Scheduled 16 February 2023

* Corresponding author: Chongqing Jiao (cqjiao@ncepu.edu.cn).

[1] State Key Laboratory of Advanced Power Transmission Technology (State Grid Smart Grid Research Institute Co. Ltd.), Changping District, Beijing 102209, China. [2] School of Electrical and Electronic Engineering, North China Electric Power University, Beijing 102206, China. [3] State Grid Zhejiang Electric Power Co., LTD. Research Institute, Hangzhou, Zhejiang Province 310014, China.

averaging method and surface impedance method [15]. In [16], the approximate simulation of the shielding effectiveness of a rectangular box with a grid wall is studied, where the holes of the grid are replaced by magnetic dipoles, and the inside of the enclosure is regarded as a piece of a waveguide.

Different from [16], this article focuses on the rectangular metallic box with all its walls perforated periodical holes. This type of shielding box has better ventilation capacity and lighter weight. We only investigate the case of low-frequency magnetic shielding. In this case, the box is electrically small. Similarly, the solution is also obtained by the combination of two submodels: the finite conductivity box with the holes covered and the perfect conductor box with the holes present. The first submodel is solved using existing approximate formulae. For the second submodel, we propose an approximate simulation technique by replacing each hole with a magnetic dipole. Then, the fields due to hole leakage are obtained by superimposing them from the dipoles and their images.

The contribution of this paper is to propose approximate analytical methods for calculating the low-frequency magnetic shielding of shielding boxes with periodical apertures. This method is a comprehensive application of some existing basic methods, including the coupling theory for small apertures, the method of images, the surface impedance method, and the shape factor based method. Furthermore, the validity of the proposed method is verified by comparisons with the finite element (FEM) simulation.

This paper is organized as follows. Section 2 introduces the approximate analytical models. In Section 3, the model is verified by comparison with finite element simulations. Finally, the conclusions are summarized in Section 4.

2. THE ANALYTICAL MODEL

2.1. The Problem Description

Figure 1(a) shows a rectangular metallic box of dimensions $a \times b \times c$ and thickness Δ, and there are square periodic unit cells with side length $d \times d$ on the six surfaces of the box. A circular hole with a radius r is opened in the middle of each unit cell to form a periodic aperture array. For the metallic material, the electrical conductivity is σ, and the relative permeability is μ_r.

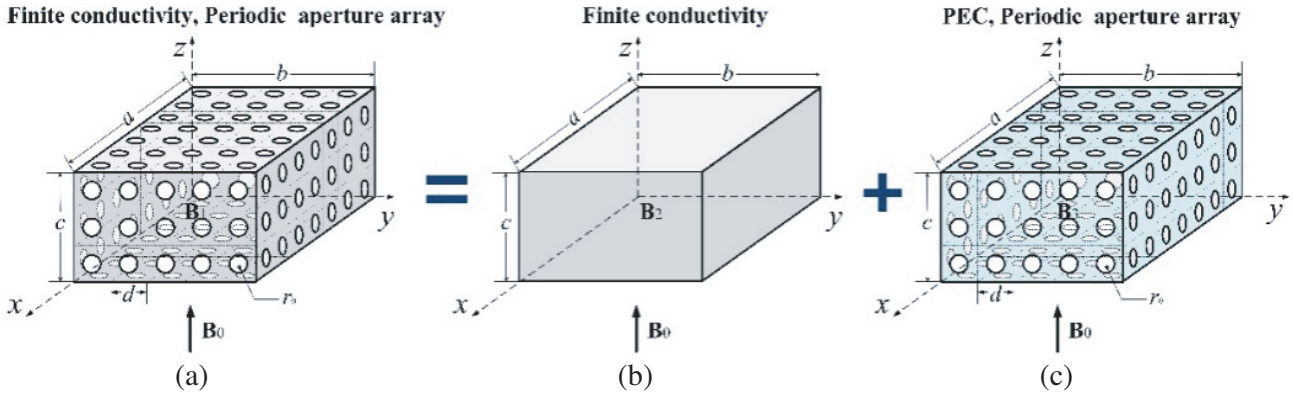

Figure 1. The shielding problem of a rectangular shielding box against an applied uniform magnetic field: (a) the rectangular box with periodic aperture array and finite conductivity, (b) the closed rectangular box with finite conductivity, and (c) the PEC rectangular box with periodic holes.

The applied uniform magnetic field $\mathbf{B}$ is along the positive z-axis. The field inside the enclosure is denoted by $\mathbf{B}_1$. As aforementioned, the original problem is divided into two sub-problems: the closed rectangular box with finite conductivity (Fig. 1(b)) and the perfect electric conductor (PEC) box with periodic holes (Fig. 1(c)). The field inside the box is represented by $\mathbf{B}_2$ and $\mathbf{B}_3$ for the two submodels, respectively. In our approximate technique, we assume that $\mathbf{B}_1$ is approximately the sum of $\mathbf{B}_2$ and $\mathbf{B}_3$: $\mathbf{B}_1 = \mathbf{B}_2 + \mathbf{B}_3$.

The SE of the rectangular box with a periodic aperture is defined as

$$\mathrm{SE}_{1,2,3} = 20\log_{10}|\mathbf{B}_0/\mathbf{B}_{1,2,3}| \tag{1}$$

wherein, SE_1, SE_2, and SE_3 denote the SE of the apertured box with finite conductivity (Fig. 1(a)), closed box (Fig. 1(b)), and apertured PEC box (Fig. 1(c)), respectively.

2.2. The Submodel for Closed Box

For the first submodel where the shape is rectangular, there is no exact analytical solution. In fact, exact analytical solutions apply only to both spherical and cylindrical shapes. Even so, with the equivalent shape factor, the SE for an arbitrarily closed shield can be approximately estimated by [17, 18]

$$\mathrm{SE}_2 = 20\log_{10}\left|\frac{\mathbf{B}_0}{\mathbf{B}_2}\right| = \begin{cases} 1+\dfrac{j\omega\mu_0\sigma V\Delta}{A} & \Delta \ll \delta \\ \left(1+\dfrac{\gamma V}{\mu_r A}\right)\dfrac{e^{\gamma\Delta}}{2} & \Delta \gg \delta \end{cases} \tag{2}$$

wherein, μ_0 is the vacuum permeability, μ_r the relativity permeability, σ the electrical conductivity, ω the angular frequency, $\gamma \approx \sqrt{j\omega\mu_0\mu_r\sigma} = (1+j)/\delta$ the propagation constant with $\delta = \sqrt{2/(\omega\mu_0\mu_r\sigma)}$ the skin depth, $V = abc$ the volume, and $A = 2(ab+bc+ca)$ the surface area of the box.

2.3. The Submodel for the PEC Box with Periodical Holes

For this submodel, we employ two approximate methods.

2.3.1. The Method of Images

First, the coupling between adjacent apertures is neglected, and then each hole can be treated individually [15, 19, 20]. The total field due to all the hole leakage is the sum of them corresponding to each hole. So, attention now is turned to a PEC rectangular shield with only one hole, as shown in Fig. 2.

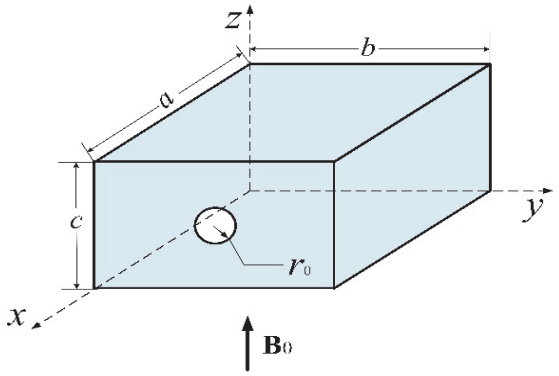

Figure 2. The PEC rectangular shielding box with a circle hole.

According to Bethe's theory [21], the penetration of the magnetic field through an electrically-small hole could be replaced with an equivalent magnetic dipole placed at the center of the hole and meanwhile, and the hole is filled completely. The magnetic dipole moment $\mathbf{m}$ is related to the tangential component of the applied field ($\mathbf{H}_t$) by the polarization coefficient α_m

$$\mathbf{m} = \alpha_m \mathbf{H}_t \tag{3}$$

The polarization coefficient of the circular aperture is [21]

$$\alpha_m = -4r_0^3/3 \tag{4}$$

For the configuration shown in Fig. 2, the moment is zero for holes in both the top and bottom surfaces, since the applied field is perpendicular to the two surfaces. In contrast, it is not zero for the other four surfaces.

Now, the key is to calculate the magnetic field inside a PEC rectangular cavity when it is excited by a magnetic dipole. This is performed by the image methods described as follows. Assuming that the magnetic dipole $\mathbf{m}$ is located at $S_0(x_s, y_s, z_s)$, then there are eight series of mirror dipoles at $(2ka+\varepsilon_x x_s, 2nb+\varepsilon_y y_s, 2pc+\varepsilon_z z_s)$. Where, $\varepsilon_x = 1$ or -1, $\varepsilon_y = 1$ or -1, and $\varepsilon_z = 1$ or -1. And k, n, and p all are integers, varying from $-\infty$ to $+\infty$. The image dipole has the same moment as the original dipole when $\varepsilon_x = 1$, and the opposite moment when $\varepsilon_x = -1$. Once the images are determined, the corresponding fields can be calculated easily as the superimposition of the field from these images. For low-frequency applications, the quasi-static condition can be well satisfied, and hence the fields from each dipole are expressed as those from a static dipole with the same dipole moment.

2.3.2. The Surface Impedance Method

Usually, not only the box is electrically small, but also the size of a unit cell is small compared to the dimension of the box, and then the following approximate formula based on the surface impedance is applicable [22]

$$\mathrm{SE}_3 = 20\log_{10}\left|1+\frac{j\omega\mu_0 V}{AZ_s}\right| \tag{5}$$

The surface impedance Z_s is [15]

$$Z_s = \frac{j8\pi r_0^3 Z_0}{3S\lambda_0} \tag{6}$$

wherein, Z is the free-space intrinsic impedance, λ the free-space wavelength, and $S = d^2$ the area of a unit cell.

3. RESULTS AND DISCUSSION

First, a PEC box is considered to investigate the effectiveness of the two approximate methods for the second submodel. Then, a finite-conductivity box is considered to evaluate the effectiveness of combining the two submodels.

3.1. The PEC Box

The PEC rectangular shielding box with periodic aperture array was modeled, material defined, boundary conditions added, meshing, and post-calculation processed in finite element software. Taking a periodic hole array shield with $a = b = c = 4\,\mathrm{cm}$, $d = 5\,\mathrm{cm}$, $r_0 = 2\,\mathrm{cm}$ as an example, the modeling was conducted in the finite element based on the software COMSOL [23]. The box was set as "Magnetic Insulation", which means that the normal magnetic field is zero on the surface of the box. An"Infinite Element Domain" boundary condition with a radius of 80 cm was set outside the box, as shown in Fig. 3(a). The number of grids is 144635 with adaptive mesh generation. The applied external magnetic field is $\mathbf{B}_0 = 0.01\mathbf{e}_z$ T. It can be seen from Fig. 3(b) that the magnetic field inside the shield is uniformly distributed except for the region very close to the surface of the shield, wherein the colorful cloud contour represents the magnitude of flux density, and the red solid lines denote the magnetic induction lines. The calculation time consumption for $f = 1\,\mathrm{MHz}$ is 14 hours with the ordinary computer with a CPU 1.6 GHz and RAM of 8 G. The higher the frequency, the longer the calculation time. In contrast, the calculation time is only 20 seconds for the proposed approximate analytical formulation.

In Fig. 4, the analytical results (the image method) of the PEC box with periodic aperture array are compared with 3D FEM simulations. Meanwhile, the results from the surface impedance method are also provided. In contrast, the surface impedance method has about 4 dB–15 dB deviation relative to the FEM simulations, while the image method has a deviation about 7 dB or less. As the hole radius gradually decreases to 1 mm, the deviation becomes obvious. The underlying reason may be that such

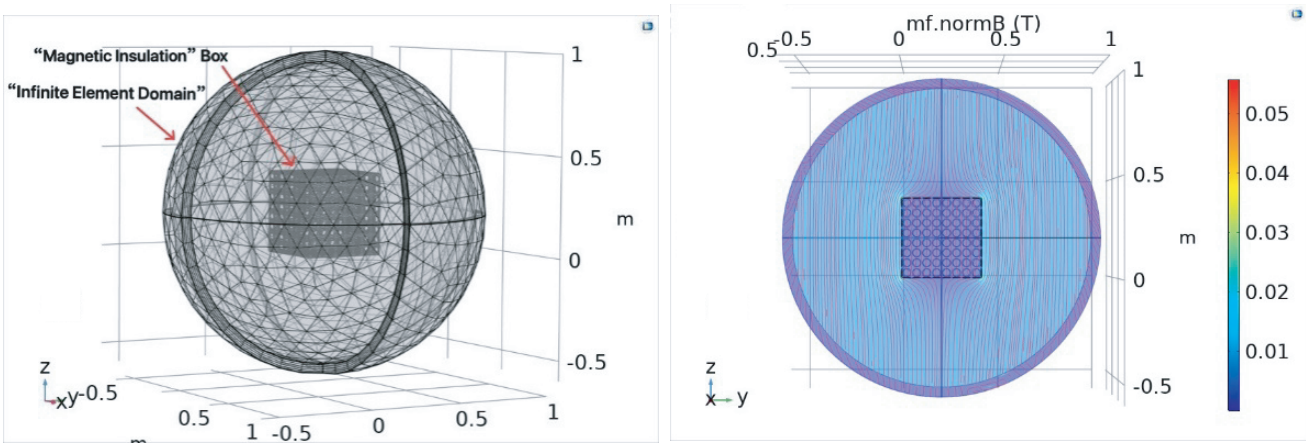

(a) (b)

Figure 3. The finite element model of the PEC rectangular box in the COMSOL software. (a) The meshing of the model: the box was set as "Magnetic Insulation" material and an "Infinite Element Domain" boundary condition with a radius of 80 cm was set outside the box. (b) The applied external magnetic field is set to $\mathbf{B}_0 = 0.01\mathbf{e}_z$ T the colorful cloud contour represents the flux density and the red solid lines denote the magnetic induction lines.

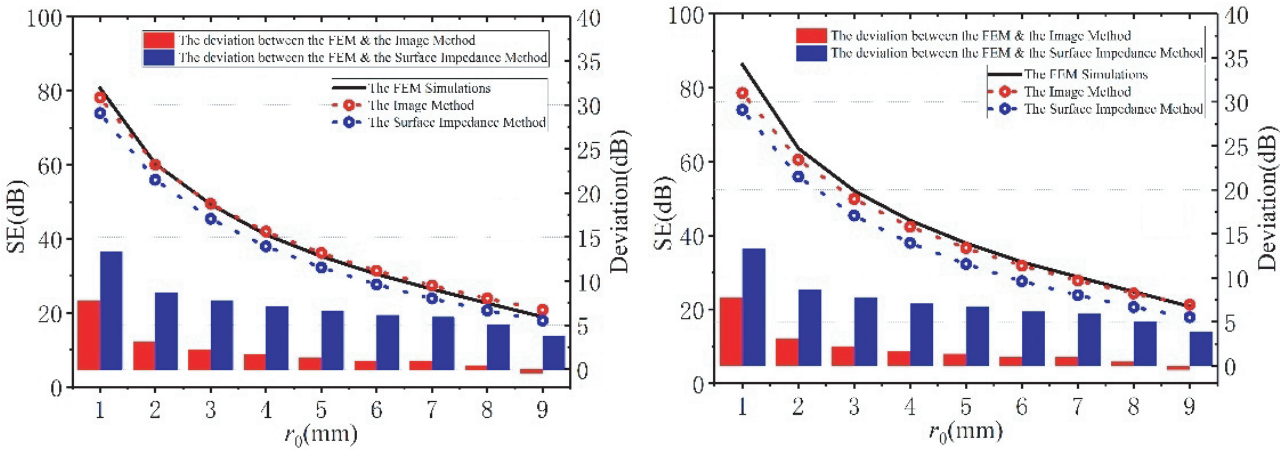

(a) (b)

Figure 4. The SE of PEC rectangular shielding box with periodic aperture array: comparisons of analytical results with FEM simulations: (a) $a = b = c = 10\,\text{cm}$, $d = 2\,\text{cm}$, (b) $a \times b \times c = 14\,\text{cm} \times 10\,\text{cm} \times 6\,\text{cm}$, $d = 2\,\text{cm}$. The dotted line, the dashed line, and the solid line are obtained by the method of images, the FEM simulation, and the surface impedance method, respectively. The red and blue bars represent the deviation between the FEM simulations and the method of images and that between the FEM simulations and the surface impedance method, respectively.

a small hole leads to tiny grid size and high non-uniformity of grid distribution around the holes, which then may affect the accuracy of numerical calculation.

It should be noted that the field distribution inside the box is approximately uniform since the holes uniformly distribute on the whole surface of the box. As a result, the SE value is independent of the position of the observation point if only the point is not near the holes. Typically, the distance between the observation point of interest and the wall is at least two times larger than the hole radius, where the field distribution is basically uniform.

3.2. An Aluminum Box

Next, an aluminum box with conductivity $\sigma = 3.774 \times 10^7$ S/m and relative permeability $\mu_r = 1$ is considered. The box is cubic with $a = b = c = 20$ cm and $\Delta = 1$ mm. Fig. 5 shows the dependence of SEs on the frequency for different aperture radii (r_0) and unit cell size, wherein the solid lines (labeled with subscript 1) correspond to the configuration of a finite-conductivity wall with holes. The dashed lines (labeled with subscript 2) refer to the configuration of a finite-conductivity wall with holes filled, and the dotted lines (labeled with subscript 3) denote the configuration of the PEC box with holes. SE_1, SE_2, and SE_3 are obtained by FEM simulations. SE_1', SE_2', and SE_3' are calculated by the approximate method for a closed box (Eq. (2)) and the method of images, respectively. SE_3'' is the result of the surface impedance method.

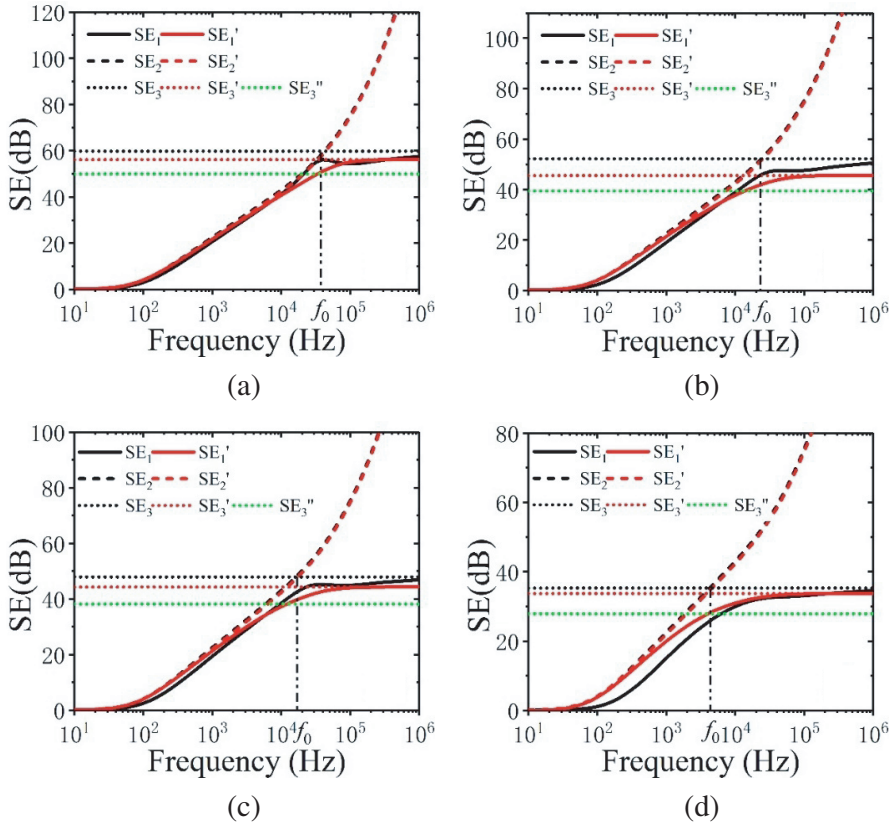

Figure 5. The SE curves of a cubic aluminum box with $a = b = c = 20$ cm and $\Delta = 1$ mm: (a) $d = 1$ cm, $r_0 = 2$ mm, (b) $d = 1$ cm, $r_0 = 3$ mm, (c) $d = 2$ cm, $r_0 = 5$ mm, (d) $d = 2$ cm, $r_0 = 7.5$ mm. Wherein, the solid lines (labeled with subscript 1) correspond to the configuration of a finite-conductivity wall with holes, the dashed lines (labeled with subscript 2) refer to the configuration of a finite-conductivity wall with holes filled, and the dotted lines (labeled with subscript 3) denotes the configuration of the PEC box with holes. The SE_1, SE_2 and SE_3 are obtained by FEM simulations. The SE_1', SE_2' and SE_3' are calculated by our approximate solution, Equation (2) and the image method, respectively. And SE_3'' is the result of the surface impedance method.

Taking Fig. 5(a) as an example, the frequency of the intersection of the SE_2 curve and SE_3 curve is defined as the critical frequency f. When the frequency is lower than the critical frequency, the curve of SE_1 basically coincides with SE_2, and the penetration of the magnetic field through metal is much greater than that through the holes. The shielding effectiveness is hardly affected by the size of the hole radius and hole-to-hole distance. Conversely, when the frequency is above the critical frequency, the curve of SE_1 basically coincides with SE_3, and the field leakage through the holes is primary.

Meanwhile, the SE is also independent of frequency but is affected obviously by the size of the hole radius and hole-to-hole distance.

It should be pointed out that when the frequency continues to increase, the shielding effectiveness will change with the frequency. For example, the FEM results within the 10 Hz–100 MHz frequency range for the PEC model are shown in Fig. 6. The results exhibit that the SE can keep unchanged if only the frequency is below about 100 MHz. Hence, the frequency-independent SE is feasible for frequencies satisfying the electrically small size condition (smaller than 1/10 wavelength). That is, the size of the box is smaller than one-tenth of the wavelength. A similar phenomenon was also observed in [24], where it was shown that for a shield with a size of about 2 m, its SE-frequency curve began to rise when the frequency exceeded about 10 MHz. Here, higher frequencies are not simulated, due to the huge burden of computation time exceeding one day for one frequency point.

For the SE results displayed in Fig. 5, here the deviation of FEM results relative to the approximate analytical results is shown in Fig. 7. Our approximate results (SE′) based on the method of images agree well with the FEM simulations (SE) with the deviation less than 6 dB in most cases. The deviation is larger when the frequency is close to the aforementioned critical frequency f_0. In contrast, the approximate results (SE′) based on the surface impedance have a deviation up to about 15 dB.

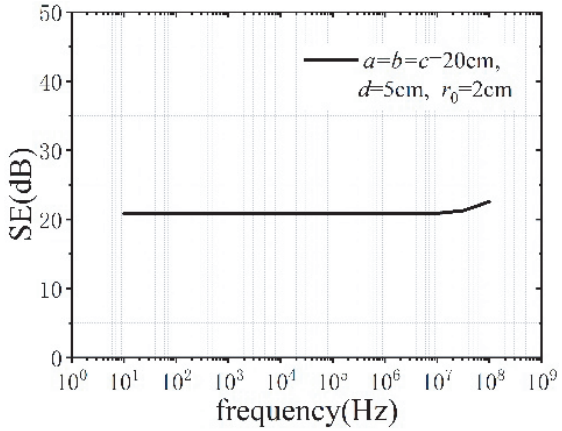

Figure 6. The SE_3 of the aluminum box with different geometric configurations within the frequency range of 10 Hz–100 MHz. The results are obtained by the FEM simulation.

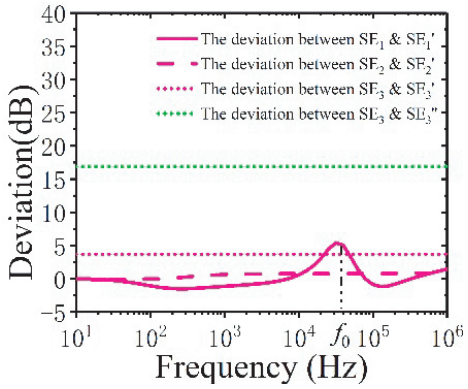

Figure 7. For the SE results displayed in Fig. 5, here the deviation of FEM results relative to the approximate analytical results is shown.

4. CONCLUSION

For a conducting rectangular shielding box with a periodic hole array in a uniform time-harmonic magnetic field, the magnetic field inside the box can also be expressed as the superposition of two analytical solutions: the finite-conductivity box with the holes covered and the PEC box with the periodic hole array. The first submodel represents the diffusion effect of magnetic field penetration through the conducting wall, and the second one denotes the aperture effect of magnetic field leakage through the aperture. The total magnetic field is the superposition of these from the two submodels. Then, an approximate solution to the SE of the second submodel is proposed, where both Bethe's small hole coupling theory and the image method are employed. A comparison with FEM simulations verified the validation of the approximate solution. Compared to the FEM simulations, the deviation of the method of images is smaller than 7 dB, but the deviation of the surface impedance method is about 5–15 dB. The results also show below the critical frequency. The SE is mainly determined by the magnetic diffusion inside the conducting wall and is gradually enhanced with the increase of the frequency. Above the critical frequency, the SE is mainly determined by the magnetic field leakage from the holes and is frequency-independent. Moreover, the hole radius and hole-to-hole distance only affect the SE for frequencies above the critical frequency.

ACKNOWLEDGMENT

This work was supported by the State Grid Corporation of China (SGCC). Project No. 5500-202119100A-0-0-00.

REFERENCES

1. Frikha, A., M. Bensetti, F. Duval, et al., "A new methodology to predict the magnetic shielding effectiveness of enclosures at low frequency in the near field," *IEEE Transactions on Magnetics*, Vol. 51, No. 3, 1–4, Mar. 2015.
2. Frikha, A., M. Bensetti, L. Pichon, et al., "Magnetic shielding effectiveness of enclosures in near field at low frequency for automotive applications," *IEEE Transactions on Electromagnetic Compatibility*, Vol. 57, No. 6, 1481–1490, Dec. 2015.
3. Mou, W. and M. Lu, "Research on shielding and electromagnetic exposure safety of an electric vehicle wireless charging coil," *Progress in Electromagnetics Research C*, Vol. 117, 55–72, 2021.
4. Zhou, Y., L. Zhang, S. Xiu, et al., "Design and analysis of platform shielding for wireless charging tram," *IEEE Access*, Vol. 7, 129443–129451, Sep. 2019.
5. Lee, S., D.-H. Kim, Y. Cho, et al., "Low leakage electromagnetic field level and high efficiency using a novel hybrid loop-array design for wireless highpower transfer system," *IEEE Transactions on Industrial Electronics*, Vol. 66, No. 6, 4356–4367, Jun. 2019.
6. Lu, C., X. Huang, C. Rong, et al., "Shielding the magnetic field of wireless power transfer system using zero-permeability metamaterial," *The Journal of Engineering*, Vol. 2019, No. 16, 1812–1815, 2019.
7. Ma, D., M. Ding, J. Lu, et al., "Study of shielding ratio of cylindrical ferrite enclosure with gaps and holes," *IEEE Sensors Journal*, Vol. 19, No. 15, 6085–6092, Aug. 2019.
8. Zhao, J., J. Zhang, Z. Liu, et al., "Immunity requirements for secondary equipment with regard to switching operations of disconnectors in substations," *2016 IEEE International Conference on Power and Renewable Energy (ICPRE)*, 135–138, Oct. 2016.
9. Moser, J. R., "Low-frequency shielding of a circular loop electromagnetic field source," *IEEE Transactions on Electromagnetic Compatibility*, Vol. 9, No. 1, 6–18, Mar. 1967.
10. Lovat, G., P. Burghignoli, R. Araneo, et al., "Magnetic shielding of planar metallic screens: A new analytical closed-form solution," *IEEE Transactions on Electromagnetic Compatibility*, Vol. 62, No. 5, 1884–1888, Nov. 2020.
11. Celozzi, S., R. Araneo, and G. Lovat, *Electromagnetic Shielding*, John Wiley & Sons, Ltd., 2008.
12. Mohammadi, E., P. Dehkhoda, A. Tavakoli, et al., "Shielding effectiveness of a metallic perforated enclosure by mesh-free method," *IEEE Transactions on Electromagnetic Compatibility*, Vol. 58, No. 3, 758–765, Jun. 2016.
13. Achkar, G. A., L. Pichon, M. Bensetti, and L. Daniel, "Homogenization of metal grid reinforced composites for near-field low frequency magnetic shielding," *Progress In Electromagnetics Research M*, Vol. 99, 153–163, 2021.
14. Yang, X. C., Z. X. Zhang, F. Ning, et al., "Shielding effectiveness analysis of the conducting spherical shell with a circular aperture against low frequency magnetic fields," *IEEE Acess*, Vol. 8, 79844–79850, Apr. 2020.
15. Bai, W. X., F. Ning, X. C. Yang, et al., "Low frequency magnetic shielding effectiveness of a conducting plate with periodic apertures," *IEEE Transactions on Electromagnetic Compatibility*, Vol. 63, No. 1, 30–37, Feb. 2021.
16. Smedt, R. D., J. De Moerloose, S. Criel, et al., "Approximate simulation of the shielding effectiveness of a rectangular enclosure with a grid wall," *1998 IEEE EMC Symposium, International Symposium on Electromagnetic Compatibility, Symposium Record (Cat. No.98CH36253)*, 1030–1034, Aug. 1998.
17. Lee, K. and G. Bedrosian, "Diffusive electromagnetic penetration into metallicenclosures," *IEEE Transactions on Antennas Propagation*, Vol. 27, No. 2, 194–198, Mar. 1979.

18. Kelha, V., J. Pukki, R. Peltonen, et al., "Design, construction, and performance of a large-volume magnetic shield," *IEEE Transactions on Magnetics*, Vol. 18, No. 1, 260–270, Jan. 1982.
19. Park, Y. B. and H. S. Lee, "Magnetostatic field penetration into multiple annular apertures," *IEEE Transactions on Magnetics*, Vol. 46, No. 11, 3866–3869, Nov. 2010.
20. Sten, J. C.-E., "Magnetic moment and surface dipole distributions of circular holes in a conducting screen," *IEEE Transactions on Electromagnetic Compatibility*, Vol. 41, No. 4, 290–297, Nov. 1999.
21. Bethe, H. A., "Theory of diffraction by small holes," *Physical Review*, Vol. 66, No. 163, Jan. 1944.
22. Casey, K. F., "Electromagnetic shielding behavior of wire-mesh screens," *IEEE Transactions on Electromagnetic Compatibility*, Vol. 30, No. 43, 298–306, Aug. 1988.
23. COMSOL Multiphysics, https://www.comsol.asia/comsol-multiphysics, last accessed 2022/7/3.
24. Park, H. H., C. H. Hyoung, and J. H. Kwon, "Improvement of low-frequency magnetic shielding measurement using rhombic and long rectangular loop antennas," *IEEE Transactions on Electromagnetic Compatibility*, Vol. 62, No. 4, 1364–1368, Aug. 2020.